

1      Vertical Structure and Seasonal Evolution of Atmospheric Oxidizing  
2      Capacity across Urban and Rural Regions: Observational Constraints  
3      from OH Radical Production Pathways

4      Tiliang Zou<sup>a, \*</sup>, Chengzhi Xing<sup>b, \*, \*</sup>, Zhijian Tang<sup>c</sup>, Yikai Li<sup>a</sup>, Zhenyi Chen<sup>d</sup>,  
5      Xiao Liang<sup>e</sup>, Wei Tan<sup>b</sup>, Cheng Liu<sup>c, f, g, \*</sup>

6      <sup>a</sup> School of Environmental Science and Optoelectronic Technology, University of Science and  
7      Technology of China, Hefei 230026, China

8      <sup>b</sup> Key Lab of Environmental Optics & Technology, Anhui Institute of Optics and Fine Mechanics,  
9      Hefei Institutes of Physical Science, Chinese Academy of Sciences, Hefei, 230031, China

10     <sup>c</sup> Department of Precision Machinery and Precision Instrumentation, University of Science and  
11     Technology of China, Hefei 230026, China

12     <sup>d</sup> State Environmental Protection Key Laboratory of Food Chain Pollution Control, Beijing  
13     Technology and Business University, Beijing, 100048, China

14     <sup>e</sup> China National Environmental Monitoring Centre, Beijing, 100012, China

15     <sup>f</sup> Anhui Institute of Optics and Fine Mechanics, Hefei Institutes of Physical Science, Chinese  
16     Academy of Sciences, Hefei 230031, China

17     <sup>g</sup> Key Laboratory of Precision Scientific Instrumentation of Anhui Higher Education Institutes,  
18     University of Science and Technology of China, Hefei 230026, China

19

20     <sup>\*</sup> These authors contributed equally to this work.

21     *\*Corresponding to:* Chengzhi Xing (xingcz@aiofm.ac.cn); Cheng Liu (chliu81@ustc.edu.cn)

Table S1. DOAS retrieval settings for O<sub>4</sub>, HONO, HCHO and O<sub>3</sub>

Parameter	Data source	Fitting interval			
		O <sub>4</sub>	HONO	HCHO	O <sub>3</sub>
Wavelength range		338–370 nm	335–373 nm	322.5–358 nm	320–340 nm
NO <sub>2</sub>	220 K, I <sub>0</sub> * correction (SCD of 10 <sup>17</sup> molec·cm <sup>-2</sup> ); (Vandaele et al., 1998a)	√	√	√	×
NO <sub>2</sub>	298 K, I <sub>0</sub> correction (SCD of 10 <sup>17</sup> molec·cm <sup>-2</sup> ); (Vandaele et al., 1998a)	√	√	√	√
O <sub>3</sub>	223 K, I <sub>0</sub> correction (SCD of 10 <sup>18</sup> molec·cm <sup>-2</sup> ); (Serdyuchenko et al., 2014)	√	√	√	√
O <sub>3</sub>	243 K, I <sub>0</sub> correction (SCD of 10 <sup>18</sup> molec·cm <sup>-2</sup> ); (Serdyuchenko et al., 2014)	×	√	√	×
O <sub>3</sub>	293 K, I <sub>0</sub> correction (SCD of 10 <sup>18</sup> molec·cm <sup>-2</sup> ); (Serdyuchenko et al., 2014)	√	×	×	√
O <sub>4</sub>	293 K, I <sub>0</sub> correction (SCD of 3×10 <sup>43</sup> molec <sup>2</sup> ·cm <sup>-5</sup> ); (Thalman and Volkamer, 2013)	√	√	√	√
HCHO	293 K, I <sub>0</sub> correction (SCD of 5×10 <sup>15</sup> molec·cm <sup>-2</sup> ); (Orphal and Chance, 2003a)	√	√	√	√
BrO	273 K, I <sub>0</sub> correction (SCD of 10 <sup>13</sup> molec·cm <sup>-2</sup> ); (Fleischmann et al., 2004)	√	√	√	×
Ring	Ring spectra calculated with DOASIS	√	√	√	√
HONO	I <sub>0</sub> correction (SCD of 10 <sup>15</sup> molec·cm <sup>-2</sup> ); (Stutz et al., 2000)	×	√	×	×
Polynomial degree		5	5	5	5
Intensity offset		Constant	No	Constant	Constant

\* Solar I<sub>0</sub> correction, Aliwell et al.(2002).

## Section S1 Error analysis

We evaluated uncertainties in the retrieved profile products by analyzing the vertical column densities (VCDs) of trace gases (HONO, HCHO and O<sub>3</sub>) and aerosol optical depth (AOD). The main sources of uncertainty considered here were smoothing and noise errors, absorption cross-section uncertainties, errors arising from the temperature dependence of absorption cross-sections, algorithmic errors, and uncertainties related to aerosol retrievals. Each component is described below.

Smoothing and noise errors ( $\sigma_{smooth\ noise}$ ): Smoothing error (S<sub>s</sub>) reflects the limited vertical resolution of the inversion and was calculated using Eq. S1. Noise error (S<sub>n</sub>) arises from DOAS fitting uncertainty, primarily driven by measurement noise. The uncertainty in the retrieved state vector ( $\hat{S}$ ) was treated as the combined contribution of these two independent sources and quantified using Eq. S2 (Frieß et al., 2006). In this study, the total smoothing and noise uncertainty was derived from the mean profile retrieval uncertainty.

$$S_s = (AK - 1)S_a(AK - 1)^T \quad (S1)$$

$$\hat{S} = (K^T S_a^{-1} K + S_\epsilon^{-1})^{-1} \quad (S2)$$

Here,  $AK$  denotes the averaging kernel matrix, which describes the sensitivity of the retrieved state to the true atmospheric state.  $S_a$  and  $S_\epsilon$  are the covariance matrices of the a priori constraints and measurements, respectively.  $K$  is the weighting-function Jacobian matrix, representing the sensitivity of the measurements to perturbations in the state vector.

Absorption cross-section uncertainties ( $\sigma_{cross\ section}$ ): Uncertainty in the absorption cross-sections is an inherent source of retrieval error. Previous studies have shown that the resulting uncertainties propagated to VCDs and vertical profiles are comparable to the original cross-section uncertainties (Friedrich et al., 2019; Song et al., 2023). We therefore adopted the reported intrinsic uncertainties of the cross-sections directly. The uncertainties for O<sub>4</sub>, HONO, HCHO and O<sub>3</sub> were 4%, 3%, 5% and 3%, respectively (Orphal and Chance, 2003b; Paur and Bass, 1985; R and R, 2013; Vandaele et al., 1998b).

Temperature-dependent absorption cross-section uncertainties ( $\sigma_{temperature}$ ): Trace-gas absorption cross-sections vary with temperature and therefore introduce an additional source of uncertainty. This systematic error was estimated by calculating the change in cross-section magnitude per kelvin between two reference temperatures and multiplying it by the maximum temperature variation during the campaign. The measurement period (1 March to 31 August 2023) spanned spring and summer, for which a maximum temperature difference of 30 K was assumed. The resulting uncertainties for O<sub>4</sub>, HONO, HCHO and O<sub>3</sub> were approximately 10%, 2%, 6% and 13%, respectively.

Algorithmic error ( $\sigma_{algorithm}$ ): This term represents the mismatch between the measured differential slant column density (DSCDs;  $y$ ) and the simulated value ( $F(x, b)$ ). As expressed in Eq. S3, this discrepancy may arise from imperfections in the forward model, inappropriate specification of parameter  $b$ , and errors independent of forward-model parameters, such as detector noise (Wang et al., 2017).

$$\sigma_{algorithm} = y - F(x, b) \quad (S3)$$

Aerosol-retrieval-related uncertainties ( $\sigma_{aerosol}$ ): The aerosol vertical profile is a key input to trace-gas profile retrieval and strongly influences the inversion results. Uncertainties in the retrieved aerosol extinction profile propagate directly into the trace-gas VCDs. This contribution was quantified using Eq. S4.

$$\sigma_{aerosol} = \sqrt{(\sigma_{smooth\ noise})^2 + (\sigma_{cross\ section})^2 + (\sigma_{temperature})^2 + (\sigma_{algorithm})^2} \quad (S4)$$

The total uncertainty for each trace gas was then derived by Gaussian error propagation, as given in Eq. S5.

$$\sigma_{total} = \sqrt{(\sigma_{smooth\ noise})^2 + (\sigma_{cross\ section})^2 + (\sigma_{temperature})^2 + (\sigma_{aerosol})^2 + (\sigma_{algorithm})^2} \quad (S5)$$

Using the framework described above, the estimated uncertainties for trace gases (HONO, HCHO and O<sub>3</sub>) and AOD are summarized in Table S1.

Table S1. Mean uncertainty estimates for trace gases and AOD (%)

	AOD	VCD		
		HONO	HCHO	O <sub>3</sub>
$\sigma_{smooth\ noise}$	5	16	27	8
$\sigma_{cross\ section}$	4	2	5	3
$\sigma_{temperature}$	10	2	6	13
$\sigma_{algorithm}$	8	11	11	5
$\sigma_{aerosol}$	/	14	14	14
Total	14	24	33	22

## Section S2 Direct emission of HONO

When analyzing the secondary formation of HONO, its direct emissions should be considered. Following the classical methods used in previous studies (Kramer et al., 2020; Li et al., 2021; Liang et al., 2017), the direct emission of HONO can be evaluated using the following equations S6 and S7.

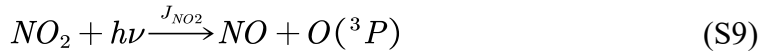
$$HONO_{emission} = NO_x \times 0.79\% \quad (S6)$$

$$HONO_{corr} = HONO_{meas} - HONO_{emission} \quad (S7)$$

The corrected HONO ( $HONO_{corr}$ ) equals the measured HONO ( $HONO_{meas}$ ) minus directly emitted HONO ( $HONO_{emission}$ ). NO<sub>x</sub> data acquisition is described in detail below. In addition, the direct emission contribution was estimated from the linear relationship between  $\Delta HONO$  and  $\Delta NO_x$  (Fig. S3), and showed a strong correlation ( $R = 0.75$ ), and the mean value of  $\Delta HONO / \Delta NO_x$  was  $0.79\% \pm 0.54\%$ . Therefore, direct HONO emissions can be obtained from the product of NO<sub>x</sub> and the emission factor (0.79%).

In this study, NO<sub>x</sub> could not be measured directly. Only NO<sub>2</sub> data were available from CNEMC, while O<sub>3</sub> data were also accessible. To obtain NO<sub>x</sub> data, we applied methods reported in previous studies (Mannschreck et al., 2004; Shetter et al., 1983), as described below.

During daytime, under sunlight, NO, NO<sub>2</sub>, and O<sub>3</sub> rapidly reach quasi-steady state (photostationary state) through the following fast reversible reactions:



Under typical urban atmospheric conditions (within a few minutes), this cycle can be approximately considered at steady state, and the concentrations of NO, NO<sub>2</sub>, and O<sub>3</sub> satisfy the following relationship:

$$[NO] = \frac{J_{NO_2}}{k} \times \frac{[NO_2]}{[O_3]} \quad (S10)$$

where [NO], [NO<sub>2</sub>], and [O<sub>3</sub>] represent the concentrations of NO, NO<sub>2</sub>, and O<sub>3</sub>, respectively;  $J_{NO_2}$  is the photolysis frequency of NO<sub>2</sub>; and  $k$  is the reaction rate constant of NO with O<sub>3</sub> (Eq. S8), calculated using the Arrhenius equation (Eq. S11) as a temperature-dependent value:

$$k(T) = A \cdot e^{-E_a/(RT)} \quad (S11)$$

Daytime NO concentrations were estimated from the NO–NO<sub>2</sub>–O<sub>3</sub> photostationary-state relationship. To minimise uncertainty, only data collected between 11:00 and 15:00 were used.

The derived NO concentrations were then combined with CNEMC NO<sub>2</sub> observations to obtain NO<sub>x</sub>. The linear relationship between  $\Delta HONO$  and  $\Delta NO_x$  was subsequently used to estimate the emission factor, yielding an emission factor

118  $\Delta HONO / \Delta NO_x$  ratio of 0.79%.

119

### Section S3 Separation of Primary and Secondary Sources of HCHO

Ground-level CO and Ox (O<sub>3</sub>+NO<sub>2</sub>) serve as tracers to isolate primary and secondary HCHO sources via a multiple linear regression framework (Hua et al., 2023; Li et al., 2024; Lin et al., 2022).

$$[HCHO] = \beta_0 + \beta_1 \times [CO] + \beta_2 \times [O_X] \quad (S12)$$

In this equation, [HCHO], [CO], and [O<sub>x</sub>] denote the measured concentrations of HCHO, CO, and O<sub>x</sub>, respectively. HCHO data are acquired from ground-based hyperspectral observations, whereas CO and O<sub>x</sub> data originate from national monitoring networks. The coefficients  $\beta_0$ ,  $\beta_1$ , and  $\beta_2$  are derived from the regression fit:  $\beta_0$  represents the background HCHO concentration,  $\beta_1$  quantifies the emission ratio of HCHO to CO (primary source), and  $\beta_2$  reflects the photochemically generated fraction of HCHO (secondary source).

The relative contributions of HCHO's background ( $P_{bg}$ ), primary ( $P_{pri}$ ), and secondary ( $P_{sec}$ ) sources are then calculated as:

$$P_{bg} = \frac{\beta_0}{\beta_0 + \beta_1 \times [CO] + \beta_2 \times [O_X]} \times 100\% \quad (S13)$$

$$P_{pri} = \frac{\beta_1 \times [CO]}{\beta_0 + \beta_1 \times [CO] + \beta_2 \times [O_X]} \times 100\% \quad (S14)$$

$$P_{sec} = \frac{\beta_2 \times [O_X]}{\beta_0 + \beta_1 \times [CO] + \beta_2 \times [O_X]} \times 100\% \quad (S15)$$

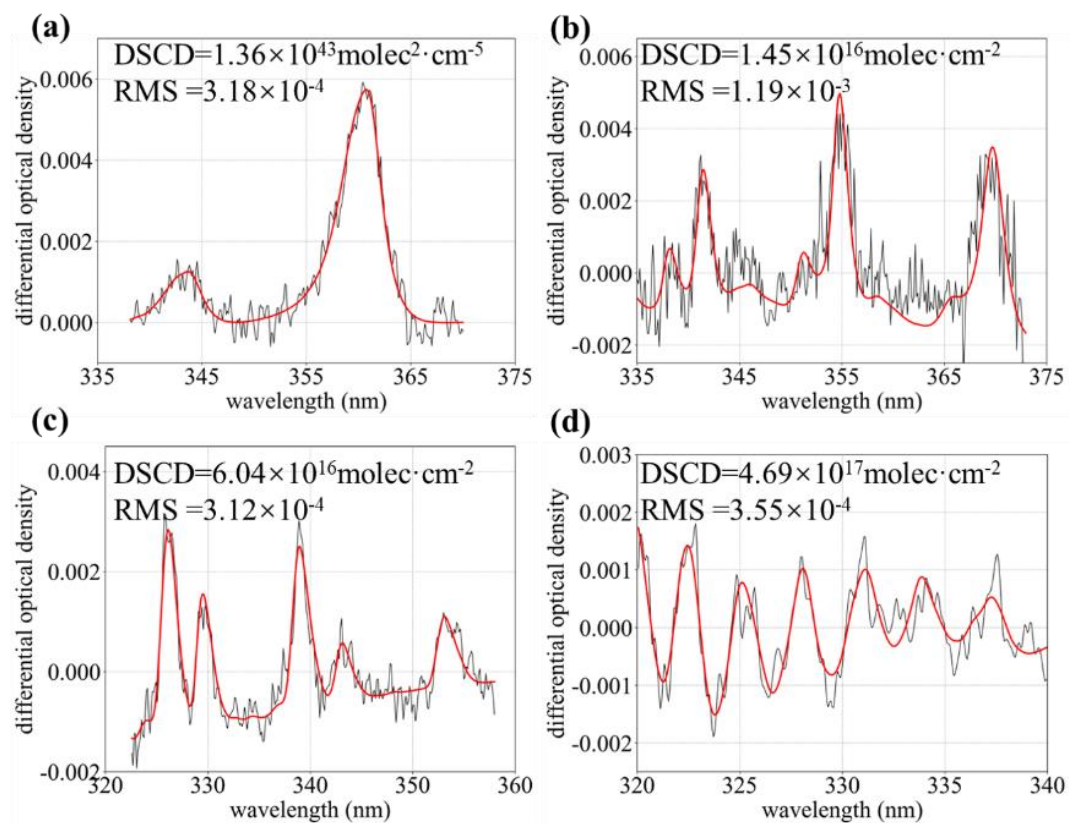


Figure S1. Representative DOAS spectral fits and fitting residuals for (a)  $O_4$ , (b) HONO, (c) HCHO and (d)  $O_3$ .



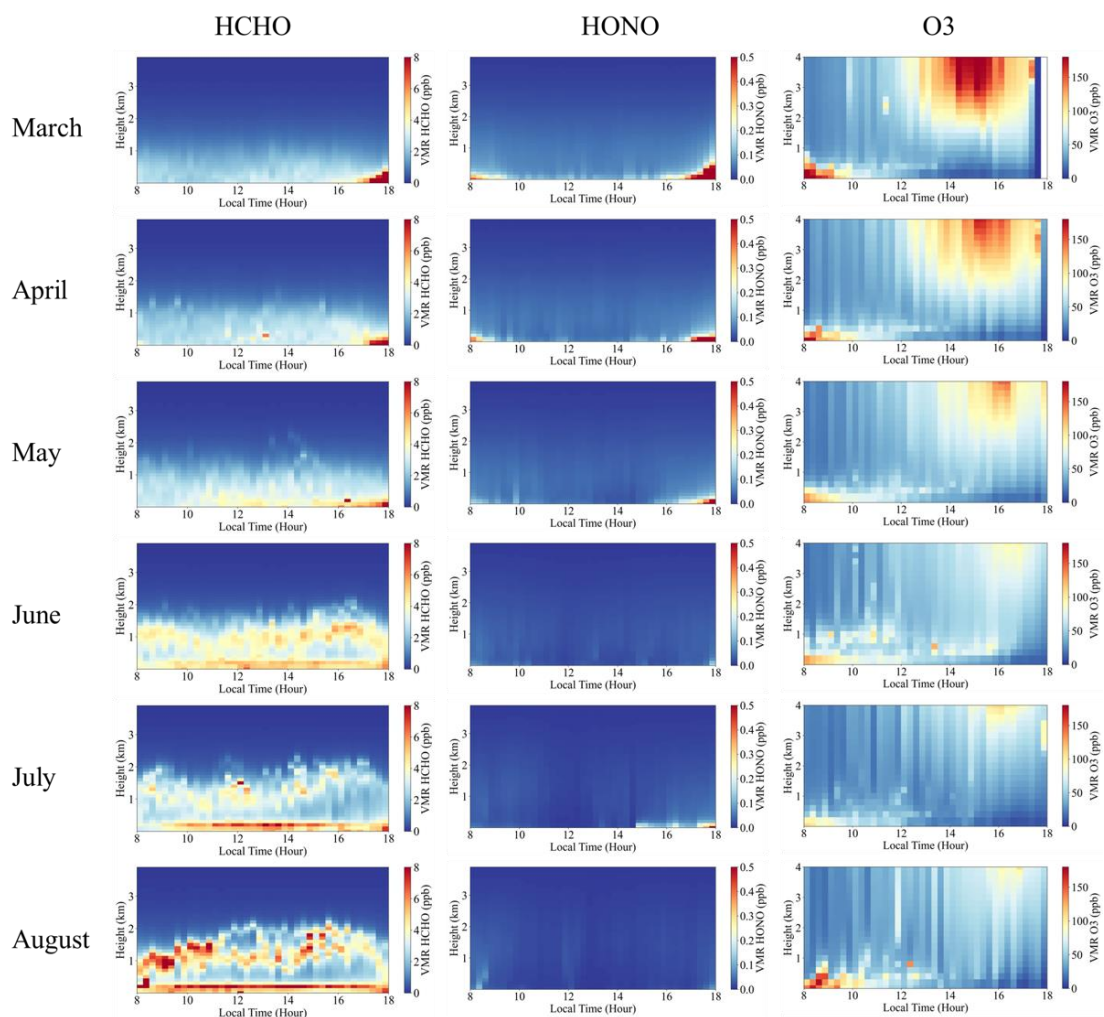


Figure S2. Monthly mean vertical profiles at AHU.

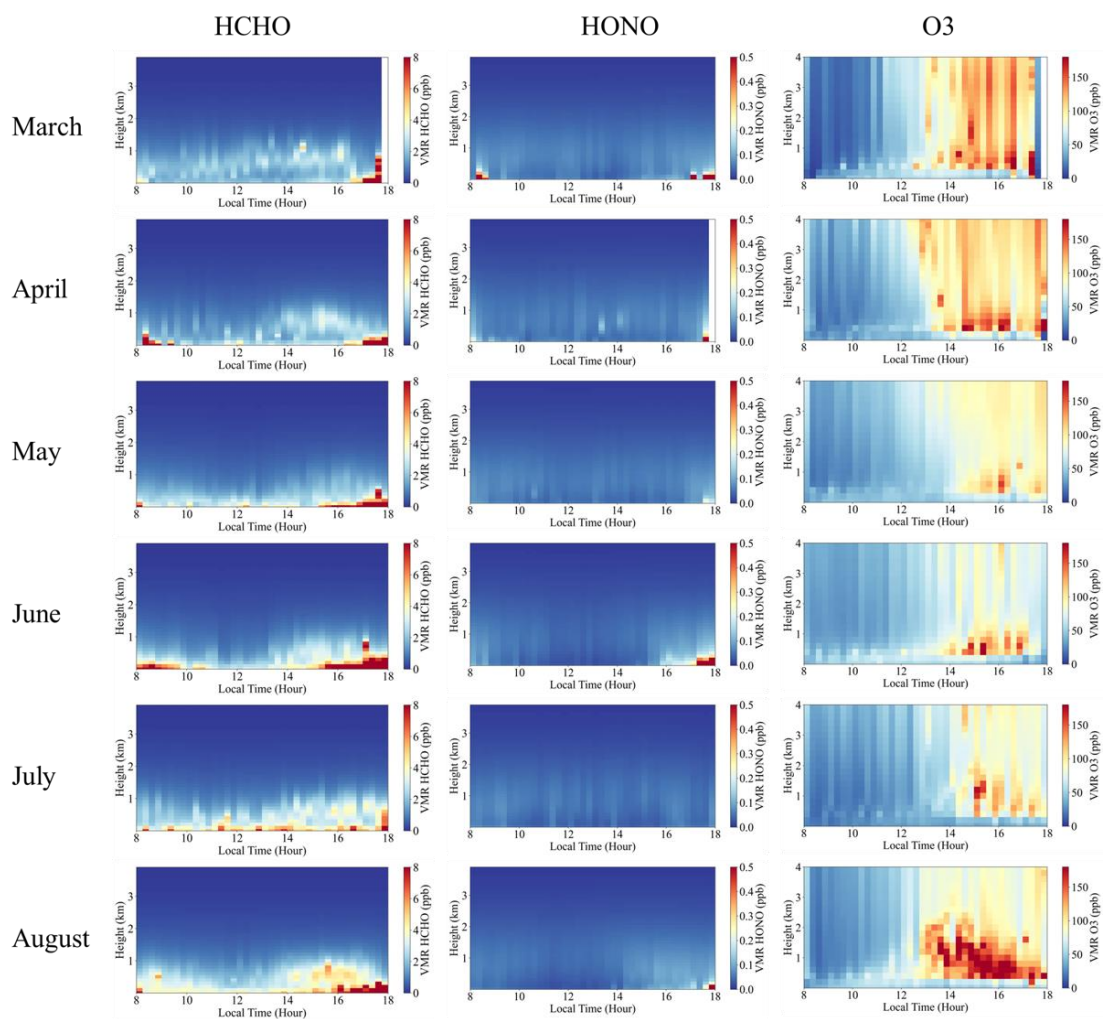
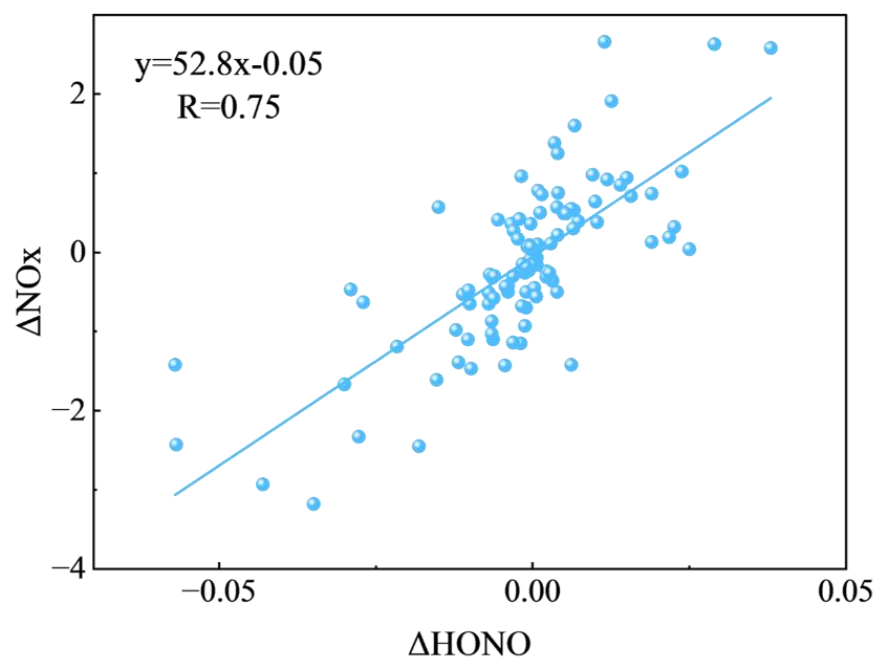


Figure S3. Monthly mean vertical profiles at CF.



147

148

Figure S4. Correlation between  $\Delta HONO$  and  $\Delta NO_x$

149

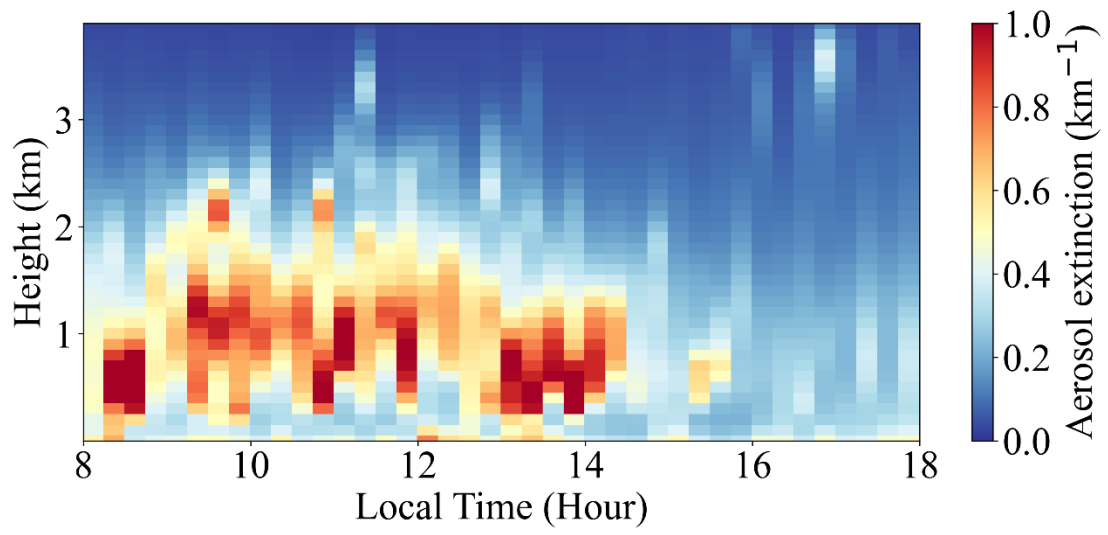


Figure S5. Vertical aerosol profiles for summer at AHU.

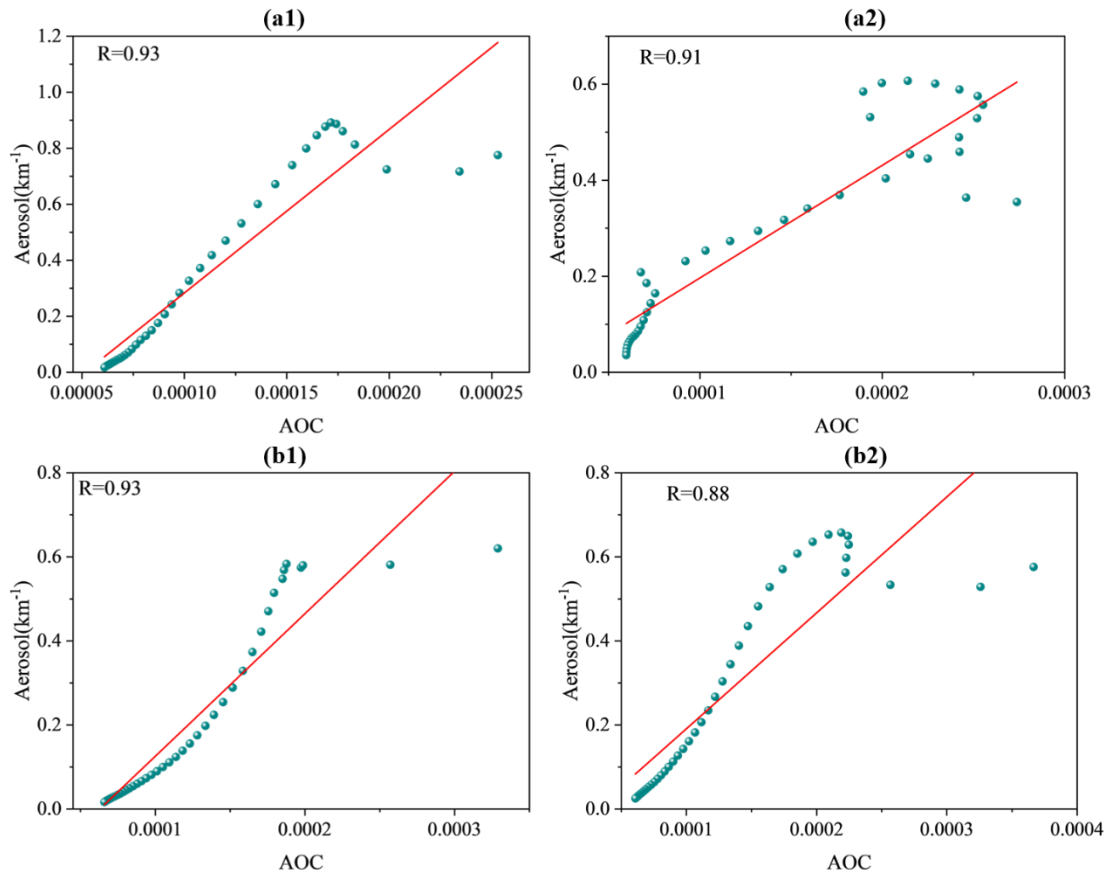


Figure S6. Correlations between AOC and aerosol. The upper row is for AHU, the lower row for CF, the left column for spring, and the right column for summer.

## References

- Aliwell, S. R., Van Roozendaal, M., Johnston, P. V., Richter, A., Wagner, T., Arlander, D. W., Burrows, J. P., Fish, D. J., Jones, R. L., Tørnkvist, K. K., Lambert, J.-C., Pfeilsticker, K., and Pundt, I.: Analysis for BrO in zenith-sky spectra: An intercomparison exercise for analysis improvement, *Journal of Geophysical Research: Atmospheres*, 107, ACH 10-1-ACH 10-20, <https://doi.org/10.1029/2001JD000329>, 2002.
- Fleischmann, O. C., Hartmann, M., Burrows, J. P., and Orphal, J.: New ultraviolet absorption cross-sections of BrO at atmospheric temperatures measured by time-windowing Fourier transform spectroscopy, *Journal of Photochemistry and Photobiology A: Chemistry*, 168, 117–132, <https://doi.org/10.1016/j.jphotochem.2004.03.026>, 2004.
- Friedrich, M. M., Rivera, C., Stremme, W., Ojeda, Z., Arellano, J., Bezanilla, A., García-Reynoso, J. A., and Grutter, M.: NO<sub>2</sub> vertical profiles and column densities from MAX-DOAS measurements in Mexico City, *Atmospheric Measurement Techniques*, 12, 2545–2565, <https://doi.org/10.5194/amt-12-2545-2019>, 2019.
- Frieß, U., Monks, P. S., Remedios, J. J., Rozanov, A., Sinreich, R., Wagner, T., and Platt, U.: MAX-DOAS O<sub>4</sub> measurements: A new technique to derive information on atmospheric aerosols: 2. Modeling studies, *Journal of Geophysical Research: Atmospheres*, 111, <https://doi.org/10.1029/2005JD006618>, 2006.
- Hua, J., Cui, Y., Guo, L., Li, H., Fan, J., Li, Y., Wang, Y., Liu, K., He, Q., and Wang, X.: Spatial characterization of HCHO and reapportionment of its secondary sources considering photochemical loss in Taiyuan, China, *Science of The Total Environment*, 865, 161069, <https://doi.org/10.1016/j.scitotenv.2022.161069>, 2023.
- Kramer, L. J., Crilley, L. R., Adams, T. J., Ball, S. M., Pope, F. D., and Bloss, W. J.: Nitrous acid (HONO) emissions under real-world driving conditions from vehicles in a UK road tunnel, *Atmospheric Chemistry and Physics*, 20, 5231–5248, <https://doi.org/10.5194/acp-20-5231-2020>, 2020.
- Li, S., Song, W., Zhan, H., Zhang, Y., Zhang, X., Li, W., Tong, S., Pei, C., Wang, Y., Chen, Y., Huang, Z., Zhang, R., Zhu, M., Fang, H., Wu, Z., Wang, J., Luo, S., Fu, X., Xiao, S., Huang, X., Zeng, J., Zhang, H., Chen, D., Gligorovski, S., Ge, M., George, C., and Wang, X.: Contribution of Vehicle Emission and NO<sub>2</sub> Surface Conversion to Nitrous Acid (HONO) in Urban Environments: Implications from Tests in a Tunnel, *Environ. Sci. Technol.*, 55, 15616–15624, <https://doi.org/10.1021/acs.est.1c00405>, 2021.
- Li, Y., Xing, C., Hong, Q., Jiao, P., Peng, H., Tang, Z., and Liu, C.: Ozone Formation Sensitivity at Various Altitudes: Seeking the Optimal Method for Sensitivity

196 Threshold Determination, *Environ. Sci. Technol. Lett.*, 11, 1334–1339,  
 197 <https://doi.org/10.1021/acs.estlett.4c00777>, 2024.

198 Liang, Y., Zha, Q., Wang, W., Cui, L., Lui, K. H., Ho, K. F., Wang, Z., Lee, S., and  
 199 Wang, T.: Revisiting nitrous acid (HONO) emission from on-road vehicles: A  
 200 tunnel study with a mixed fleet, *Journal of the Air & Waste Management*  
 201 *Association*, 67, 797–805, <https://doi.org/10.1080/10962247.2017.1293573>,  
 202 2017.

203 Lin, H., Xing, C., Hong, Q., Liu, C., Ji, X., Liu, T., Lin, J., Lu, C., Tan, W., Li, Q., and  
 204 Liu, H.: Diagnosis of Ozone Formation Sensitivities in Different Height Layers  
 205 via MAX-DOAS Observations in Guangzhou, *Journal of Geophysical Research:*  
 206 *Atmospheres*, 127, e2022JD036803, <https://doi.org/10.1029/2022JD036803>,  
 207 2022.

208 Mannschreck, K., Gilge, S., Plass-Duelmer, C., Fricke, W., and Berresheim, H.:  
 209 Assessment of the applicability of NO-NO<sub>2</sub>-O<sub>3</sub> photostationary state to long-term  
 210 measurements at the Hohenpeissenberg GAW Station, Germany, *Atmospheric*  
 211 *Chemistry and Physics*, 4, 1265–1277, <https://doi.org/10.5194/acp-4-1265-2004>,  
 212 2004.

213 Orphal, J. and Chance, K.: Ultraviolet and visible absorption cross-sections for  
 214 HITRAN, *Journal of Quantitative Spectroscopy and Radiative Transfer*, 82, 491–  
 215 504, [https://doi.org/10.1016/S0022-4073\(03\)00173-0](https://doi.org/10.1016/S0022-4073(03)00173-0), 2003a.

216 Orphal, J. and Chance, K.: Ultraviolet and visible absorption cross-sections for  
 217 HITRAN, *Journal of Quantitative Spectroscopy and Radiative Transfer*, 82, 491–  
 218 504, [https://doi.org/10.1016/S0022-4073\(03\)00173-0](https://doi.org/10.1016/S0022-4073(03)00173-0), 2003b.

219 Paur, R. J. and Bass, A. M.: The Ultraviolet Cross-Sections of Ozone: II. Results and  
 220 Temperature Dependence, in: *Atmospheric Ozone*, Springer, Dordrecht, 611–616,  
 221 [https://doi.org/10.1007/978-94-009-5313-0\\_121](https://doi.org/10.1007/978-94-009-5313-0_121), 1985.

222 R, T. and R, V.: Temperature dependent absorption cross-sections of O<sub>2</sub>-O<sub>2</sub> collision  
 223 pairs between 340 and 630 nm and at atmospherically relevant pressure, *Physical*  
 224 *chemistry chemical physics: PCCP*, 15, <https://doi.org/10.1039/c3cp50968k>,  
 225 2013.

226 Rodgers, C. D.: *Inverse Methods for Atmospheric Sounding - Theory and Practice*,  
 227 [https://doi.org/Inverse%20Methods%20for%20Atmospheric%20Sounding%20-](https://doi.org/Inverse%20Methods%20for%20Atmospheric%20Sounding%20-%20Theory%20and%20Practice)  
 228 [%20Theory%20and%20Practice](https://doi.org/Inverse%20Methods%20for%20Atmospheric%20Sounding%20-%20Theory%20and%20Practice), 2000.

229 Serdyuchenko, A., Gorshelev, V., Weber, M., Chehade, W., and Burrows, J. P.: High  
 230 spectral resolution ozone absorption cross-sections &ndash; Part 2: Temperature  
 231 dependence, *Atmospheric Measurement Techniques*, 7, 625–636,  
 232 <https://doi.org/10.5194/amt-7-625-2014>, 2014.

233 Shetter, R., Stedman, D., and West, D.: The NO/NO<sub>2</sub>/O<sub>3</sub> Photostationary State in  
 234 Claremont, California, Journal of the Air Pollution Control Association, 1983.

235 Song, Y., Xing, C., Liu, C., Lin, J., Wu, H., Liu, T., Lin, H., Zhang, C., Tan, W., Ji, X.,  
 236 Liu, H., and Li, Q.: Evaluation of transport processes over North China Plain and  
 237 Yangtze River Delta using MAX-DOAS observations, Atmospheric Chemistry  
 238 and Physics, 23, 1803–1824, <https://doi.org/10.5194/acp-23-1803-2023>, 2023.

239 Stutz, J., Kim, E. S., Platt, U., Bruno, P., Perrino, C., and Febo, A.: UV-visible  
 240 absorption cross sections of nitrous acid, Journal of Geophysical Research:  
 241 Atmospheres, 105, 14585–14592, <https://doi.org/10.1029/2000JD900003>, 2000.

242 Thalman, R. and Volkamer, R.: Temperature dependent absorption cross-sections of  
 243 O<sub>2</sub>–O<sub>2</sub> collision pairs between 340 and 630 nm and at atmospherically relevant  
 244 pressure, Phys. Chem. Chem. Phys., 15, 15371,  
 245 <https://doi.org/10.1039/c3cp50968k>, 2013.

246 Vandaele, A. C., Hermans, C., Simon, P. C., Carleer, M., Colin, R., Fally, S., Mérienne,  
 247 M. F., Jenouvrier, A., and Coquart, B.: Measurements of the NO<sub>2</sub> absorption  
 248 cross-section from 42 000 cm<sup>–1</sup> to 10 000 cm<sup>–1</sup> (238–1000 nm) at 220 K and  
 249 294 K, Journal of Quantitative Spectroscopy and Radiative Transfer, 59, 171–  
 250 184, [https://doi.org/10.1016/S0022-4073\(97\)00168-4](https://doi.org/10.1016/S0022-4073(97)00168-4), 1998a.

251 Vandaele, A. C., Hermans, C., Simon, P. C., Carleer, M., Colin, R., Fally, S., Mérienne,  
 252 M. F., Jenouvrier, A., and Coquart, B.: Measurements of the NO<sub>2</sub> absorption  
 253 cross-section from 42 000 cm<sup>–1</sup> to 10 000 cm<sup>–1</sup> (238–1000 nm) at 220 K and  
 254 294 K, Journal of Quantitative Spectroscopy and Radiative Transfer, 59, 171–  
 255 184, [https://doi.org/10.1016/S0022-4073\(97\)00168-4](https://doi.org/10.1016/S0022-4073(97)00168-4), 1998b.

256 Wang, Y., Lampel, J., Xie, P., Beirle, S., Li, A., Wu, D., and Wagner, T.: Ground-based  
 257 MAX-DOAS observations of tropospheric aerosols, NO<sub>2</sub>, SO<sub>2</sub> and HCHO in  
 258 Wuxi, China, from 2011 to 2014, Atmospheric Chemistry and Physics, 17, 2189–  
 259 2215, <https://doi.org/10.5194/acp-17-2189-2017>, 2017.